


The International Journal of Robotics Research

<http://ijr.sagepub.com>

The Human-size Humanoid Robot That Can Walk, Lie Down and Get Up
Hirohisa Hirukawa, Shuuji Kajita, Fumio Kanehiro, Kenji Kaneko and Takakatsu Isozumi
The International Journal of Robotics Research 2005; 24; 755
DOI: 10.1177/0278364905057217

The online version of this article can be found at:
<http://ijr.sagepub.com/cgi/content/abstract/24/9/755>

Published by:

 SAGE Publications

<http://www.sagepublications.com>

On behalf of:



Multimedia Archives

Additional services and information for *The International Journal of Robotics Research* can be found at:

Email Alerts: <http://ijr.sagepub.com/cgi/alerts>

Subscriptions: <http://ijr.sagepub.com/subscriptions>

Reprints: <http://www.sagepub.com/journalsReprints.nav>

Permissions: <http://www.sagepub.com/journalsPermissions.nav>

Hirohisa Hirukawa
Shuuji Kajita
Fumio Kanehiro
Kenji Kaneko

National Institute of Advanced Industrial
Science and Technology (AIST)
Tsukuba Central 2, 1-1-1 Umezono,
Tsukuba, Ibaraki, 305-8568 Japan

Takakatsu Isozumi

Kawada Industries, Inc.,
122-1 Hagadai, Haga, Tochigi 321-3325 Japan

The Human-size Humanoid Robot That Can Walk, Lie Down and Get Up

Abstract

In this paper we present a humanoid robot, HRP-2P, which can walk, lie down and get up. We believe that HRP-2P (154 cm height and 58 kg weight) is the first humanoid robot that is the size of a human and can lie down and get up. Biped walking is realized by a walking pattern generator using a preview control and a feedback control. The lying down and getting up motions were made possible by HRP-2P's compact body with a waist joint and a novel motion controller.

KEY WORDS—humanoid robot, biped walking, getting up motion, human-size

1. Introduction

In recent years, since Honda P2 (Hirai et al. 1998) was revealed with the astonishing response, more and more research has been carried out in the area of humanoid robotics. Honda developed P3 and ASIMO (Hirose et al. 2001) after P2, the University of Tokyo developed H6 and H7 (Kagami et al. 2001), and Sony developed small-size humanoid robots SDR-3X (Kuroki et al. 2001) and SDR-4X for entertainment applications.

The Ministry of Economy, Trade and Industry (METI) of Japan ran Humanoid Robotics Project (HRP) from 1998FY to 2003FY, which was led by Hirochika Inoue (Inoue et al. 2001). The objective of the HRP is to create humanoid robots that can perform significant tasks in real working environments. To this end, the HRP has developed a humanoid robot called

HRP-2P, which can walk, lie down and get up. We believe that HRP-2P (154 cm height and 58 kg weight) is the first humanoid robot that is the size of a human and can lie down and get up.

Biped walking is realized by a walking pattern generator based on a preview control and a feedback control composed of a posture control, a stabilizer for a rough terrain and a zero moment point (ZMP) control. Two approaches are available to generate the walking patterns. The first approach can plan the patterns to let the ZMP follow a specified trajectory; this is called the ZMP-based approach. It demands the precise dynamics model of the robot, and therefore the performance of the approach should depend on the accuracy of the model (Takanishi et al. 1990; Hirai et al. 1998; Kagami et al. 2000). The second approach plans the patterns from a partial knowledge of the model, such as the center of mass (CoM) and total angular momentum; this is called the inverted pendulum approach. Although the approach is more robust for the error of the model parameters, the generated patterns have to be tuned substantially by a feedback control since the patterns were not created from the detailed dynamics model (Sano and Furusho 1990; Kajita and Tani 1991; Pratt, Dilworth, and Pratt 1997; Kajita, Matsumoto, and Saigo 2001; Kajita et al. 2002). Since the inverted pendulum approach tries to stabilize the walking motions by modifying the foot placement dynamically, the approach cannot be applied when the feasible range of the placement is limited (e.g., the robot walks on stepping stones). Although the ZMP-based approach can plan a stable walking pattern without changing the foot placement, the complexity of the planning algorithm is too high to be computed in real time.

In this paper, we propose a novel walking pattern generator that can specify the desired foot placement with a low

computational complexity. The proposed method is a mixture of the ZMP-based approach and the inverted pendulum approach, and employs a preview controller in which the precise multibody dynamics of the robot can be taken into account.

The development of lying down and getting up motions is essential to realize useful humanoid robots as well as biped walking, since one of the weak points of a humanoid robot is that the robot may tip over. Although many researches have focused on methods to improve the stability of walking, it is impossible to prevent the robot from tipping over for its lifetime. An alternative way is to let the robot get up from the floor when it has tipped over. This is considered to be a kind of fail-safe design of a humanoid robot. Note that the robot must fall down with the minimum damage before it can get up from the floor. In other words, falling motion control must be applied to a humanoid robot for the purpose, which is also under development (Fujiwara et al. 2002).

There are several pioneering researches concerning the getting up motions of small-size humanoid robots. To the best of our knowledge, "Hanzou", developed by one of the authors and their co-workers, is the first humanoid robot that can get up by itself (Inaba et al. 1995a). It can also continue to walk even after it tips over. Hanzou has a height of 30 cm, a weight of 2 kg, and 16 degrees of freedom (DOF). When it tips over and is lying on its back, it can roll over by swinging its legs. The motion of getting up is segmented into a sequence of contact states between the robot and the floor, but each transition between consecutive states is realized by a playback of a fixed motion pattern. These patterns are designed by considering the static balance of the robot from the geometric model (Inaba et al. 1995b). Sony SDR-3X has a height of 50 cm, a weight of 5 kg, with 24 DOF, and can also get up with the robot face upward and downward in the simulator (Raibert et al. 2001) and experiments. SDR-4X, which is the successor of SDR-3X, has a height of 58 cm, a weight of 6.5 kg with 38 DOF, falls down intentionally when pushed by a human, and can get up with the face upward and downward.

In this paper, we present the first human-size humanoid robot that can lie down and get up. The motion can be realized partly because the hardware of HRP-2P has no backpack, has a waist joint, and has wide movable ranges of its joints. From the software side, the motions are also segmented into sequences of contact states between the robot and the floor as well as the method applied for Hanzou. Besides, the transitions between specific states are realized by the dynamic control of the robot whose CoM may not be above the supporting polygon. The dynamic control is essential since the human-size humanoid robot has feet of relatively smaller size compared with small-size humanoid robots.

This paper is organized as follows. In Section 2 we describe the specifications of HRP-2P. In Section 3 we present how biped walking is implemented, and in Section 4 we explain how lying and getting up motions are realized. Section 5 concludes the paper.

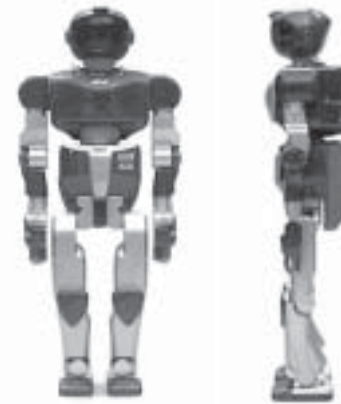


Fig. 1. HRP-2 prototype (HRP-2P).

2. Humanoid Robot HRP-2P

HRP-2P is a humanoid robot with a height of 154 cm and a weight of 58 kg, developed in the HRP (Figure 1; Kaneko et al. 2002b).

HRP-2P is designed to be a humanoid robot that can lie down and get up as well as perform biped walking. The specifications required for the motions include no backpack on the back, a waist joint that can move the upper half of the body forward and backward, and wide movable ranges of joints, each of which covers the range of the corresponding joint of a human described as follows.

2.1. Backpack Free Design

The body of HRP-2P contains the equipment required for its independent operation including computers and batteries, while some existing humanoid robots need a large backpack for them (Hirai et al. 1998; Hirose et al. 2001). The compact shape of HRP-2P has been realized mainly by a high density implementation of electronic parts.

When a humanoid robot tries to get up from the floor, various parts of the body may contact with the floor and the transitions between different contact states must be smooth to realize the motion. For example, a large projection from the body, such as a backpack, can cause difficulty for the robot when it gets up with its face upward. HRP-2P has a human-like proportion without any large projection, as shown in Figure 1.

2.2. Waist Joint

HRP-2P has a waist joint with two DOF. The joint configuration of HRP-2P is illustrated in Figure 2. The pitch joint of the waist can rotate the trunk of the robot in a large angle on the sagittal plane. The rotation enables the hand of the robot to leave the floor when the robot is supported by its hands and knees. In detail, the projection of the CoM of the robot

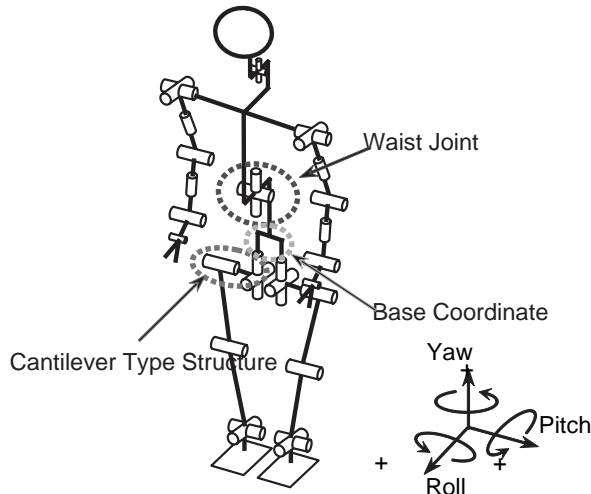


Fig. 2. Configuration of HRP-2P.

should be moved between the position of the knees and that of the feet on the sagittal plane when the hands leave the floor, and the motion makes the distance from the hand joints to the hip joints longer. Although the distance can be controlled by stretching the arms, the motion can be realized more easily by the waist joint and the arms, which should make the configuration of the arms simpler. This is the reason why HRP-2P is designed to have a waist joint.

2.3. Wide Movable Ranges of Joints

The movable range of each joint of HRP-2P was designed to include that of the corresponding joint of a standard human in the initial stage to allow the robot to make the moves which a standard human can make. Table 1(a) shows the movable ranges of the head, right arm, right hand, waist, and right leg of a standard human. However, the kinematics and dynamics of HRP-2P are significantly different from those of a standard human (e.g., HRP-2P has a much smaller number of joints than a human). Besides, the robot may be requested to perform what the human cannot perform.

Therefore, the movable ranges of the joints of HRP-2P were designed by various simulations of the motions which the robot is expected to perform. Table 1(b) shows the final ranges, which are wider than those of the corresponding joints of the human at many joints.

3. Biped Walking

We present a novel walking pattern generator that can specify the desired foot placement with a low computational com-

Table 1. Movable Ranges of Joints of a Standard Human and the Humanoid Robot HRP-2P

Joint		(a) Human	(b) HRP-2P
Head	R	−50 to 50	NA
	P	−50 to 60	−20 to 55
	Y	−70 to 70	−45 to 45
Right arm			
	Shoulder	R	−90 to 0
		P	−180 to 50
Elbow		Y	−90 to 90
		P	−145 to 0
		Y	−90 to 90
Wrist		R	−55 to 25
		P	−70 to 90
		Y	−90 to 90
Right hand		P	0 to 90
		R	−50 to 50
		P	−30 to 45
Waist		Y	−40 to 40
		R	−45 to 20
		P	−125 to 15
Right leg		Y	−45 to 45
		P	0 to 130
		R	−20 to 30
Ankle		P	−20 to 45
		R	−20 to 30
		P	−75 to 42

Units are degrees, R denotes roll axis, P denotes pitch axis, and Y denotes yaw axis.

plexity. The proposed method is a mixture of the ZMP-based approach and the inverted pendulum approach, and employs a preview controller in which the precise multibody dynamics of the robot can be taken into account. The details are described in the following.

3.1. Dynamics Model of a Biped Robot

3.1.1. Equations of Motion of a Simplified Robot

When a biped robot is supported by one leg, the dynamics of the robot can be approximated by that of a simple inverted pendulum whose foot is that of the leg and the head is the CoM of the robot with a massless telescopic leg (see Figure 3). The position of the point mass $\mathbf{p} = [x, y, z]^T$ can be uniquely specified by a set of state variables $\mathbf{q} = [\theta_r, \theta_p, r]^T$ by

$$x = r S_p, \quad (1)$$

$$y = -r S_r, \quad (2)$$

$$z = r D, \quad (3)$$

where $S_r \equiv \sin \theta_r$, $S_p \equiv \sin \theta_p$, $D \equiv \sqrt{1 - S_r^2 - S_p^2}$. Note that the x -axis points to the walking direction.

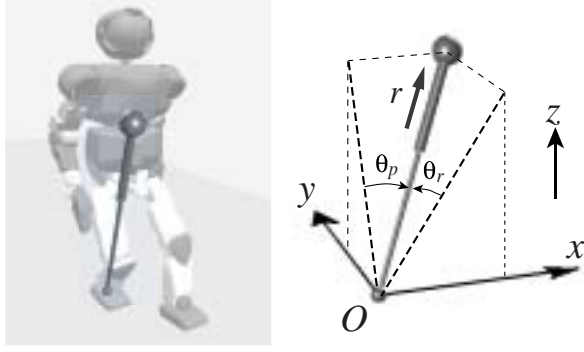


Fig. 3. The robot and 3D pendulum.

Let $[\tau_r, \tau_p, f]^T$ be the actuator torque and force associated with the state variables $[\theta_r, \theta_p, r]^T$. Then the equations of motion of the three-dimensional (3D) inverted pendulum in the Cartesian coordinates can be given by

$$m \begin{bmatrix} \ddot{x} \\ \ddot{y} \\ \ddot{z} \end{bmatrix} = (J^T)^{-1} \begin{bmatrix} \tau_r \\ \tau_p \\ f \end{bmatrix} + \begin{bmatrix} 0 \\ 0 \\ -mg \end{bmatrix}, \quad (4)$$

where m is the total mass of the robot, g is the gravity acceleration, and Jacobian J can be written by

$$J = \frac{\partial \mathbf{p}}{\partial \mathbf{q}} = \begin{bmatrix} 0 & rC_p & S_p \\ -rC_r & 0 & -S_r \\ -rC_r S_r / D & -rC_p S_p / D & D \end{bmatrix}, \quad (5)$$

$C_r \equiv \cos \theta_r, C_p \equiv \cos \theta_p.$

Multiplying eq. (4) by J^T from the left, we obtain

$$m \begin{bmatrix} 0 & -rC_r & -rC_r S_r / D \\ rC_p & 0 & -rC_p S_p / D \\ S_p & -S_r & D \end{bmatrix} \begin{bmatrix} \ddot{x} \\ \ddot{y} \\ \ddot{z} \end{bmatrix} = \begin{bmatrix} \tau_r \\ \tau_p \\ f \end{bmatrix} - mg \begin{bmatrix} -rC_r S_r \\ -rC_p S_p / D \\ D \end{bmatrix}. \quad (6)$$

The product of the first row of the equation and D/C_r yields

$$m(-rD\ddot{y} - rS_r\ddot{z}) = \frac{D}{C_r} \tau_r + rS_r mg. \quad (7)$$

Substituting the kinematic relationship of eqs. (2) and (3), we obtain the equation of translational motion along the y -axis

$$m(-z\ddot{y} + y\ddot{z}) = \tau_x - mgy, \quad (8)$$

where τ_x is the torque around the x -axis defined by

$$\tau_x \equiv \frac{D}{C_r} \tau_r.$$

Similarly, the equation of translational motion along the x -axis can be derived from the second row of eq. (6) as

$$m(z\ddot{x} - x\ddot{z}) = \tau_y + mgx, \quad (9)$$

where τ_y is the torque around the y -axis defined by

$$\tau_y \equiv \frac{D}{C_p} \tau_p.$$

3.1.2. 3D Linear Inverted Pendulum Mode

We impose an artificial constraint on the motions of the pendulum to plan the walking patterns of a biped robot. That is, the motions of the point mass of the pendulum are constrained on a plane whose normal vector is $[k_x, k_y, -1]^T$ and z intersection is z_c . The equation of the plane can be given by

$$z = k_x x + k_y y + z_c. \quad (10)$$

When the robot walks over a rough terrain on a slope, the normal vector of the constraining plane should be that of the slope and z_c is set to the average height of the CoM. Figure 4 illustrates the pendulum with the constraining plane. Taking the second-order derivatives of eq. (10), we obtain

$$\ddot{z} = k_x \ddot{x} + k_y \ddot{y}. \quad (11)$$

Substituting eqs. (10) and (11) into eqs. (8) and (9), we can derive the equations of motion of the pendulum under the constraint as

$$\ddot{y} = \frac{g}{z_c} y - \frac{k_x}{z_c} (x\ddot{y} - \ddot{x}y) - \frac{1}{mz_c} \tau_x, \quad (12)$$

$$\ddot{x} = \frac{g}{z_c} x + \frac{k_y}{z_c} (x\ddot{y} - \ddot{x}y) + \frac{1}{mz_c} \tau_y. \quad (13)$$

When the floor is a flat and horizontal plane, we set $k_x = 0, k_y = 0$ and the equations become

$$\ddot{y} = \frac{g}{z_c} y - \frac{1}{mz_c} \tau_x, \quad (14)$$

$$\ddot{x} = \frac{g}{z_c} x + \frac{1}{mz_c} \tau_y. \quad (15)$$

The equations of the motion of the pendulum for the general case can also be reduced to eqs. (14) and (15) by imposing another artificial constraint as follows. Multiplying eq. (12) by x and eq. (13) by y , respectively, and adding the products, we obtain

$$x\ddot{y} - \ddot{x}y = \frac{-1}{mz} (\tau_x x + \tau_y y). \quad (16)$$

Therefore, when τ_x and τ_y are controlled so that

$$\tau_x x + \tau_y y = 0, \quad (17)$$

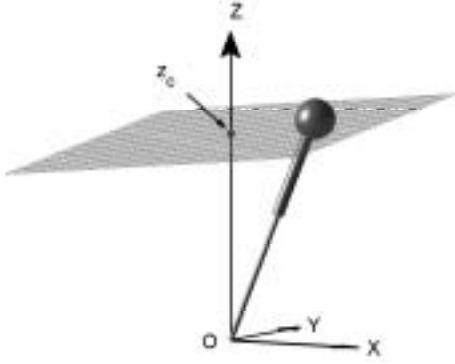


Fig. 4. A pendulum under constraint

eqs. (12) and (13) are reduced to eqs. (14) and (15). Note that no approximation has been applied in the reduction from eq. (4) to eqs. (14) and (15).

Equations (14) and (15) are independent and linear differential equations in spite of the fact that the original equations of motion are non-linear differential equations. The only parameter of the equations is z_c . We call the dynamics given by eqs. (14) and (15) the 3D linear inverted pendulum mode (3D-LIPM; Hara, Yokogawa, and Sadao 1997; Kajita, Matsumoto, and Saigo 2001).

3.1.3. ZMP Equations and Cart-table Model

For the 3D-LIPM with the horizontal constraint $k_x = k_y = 0$, the ZMP (Vukobratović and Stepanenko 1972) can be given simply by

$$p_x = -\frac{\tau_y}{mg}, \quad (18)$$

$$p_y = \frac{\tau_x}{mg}, \quad (19)$$

where (p_x, p_y) is the location of the ZMP on the floor. Substituting eqs. (18) and (19) to the 3D-LIPM (eqs. (14) and (15)), we obtain

$$\ddot{y} = \frac{g}{z_c}(y - p_y), \quad (20)$$

$$\ddot{x} = \frac{g}{z_c}(x - p_x). \quad (21)$$

The ZMP should be the outputs of the system equations to be controlled. To this end, eqs. (20) and (21) are rewritten as

$$p_y = y - \frac{z_c}{g}\ddot{y}, \quad (22)$$

$$p_x = x - \frac{z_c}{g}\ddot{x}, \quad (23)$$

and will be called the ZMP equations in the rest of the paper.

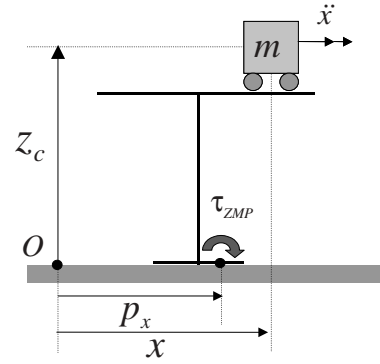


Fig. 5. A cart-table model.

Figure 5 shows a comprehensive model corresponding to the equations. A cart with mass m runs on a table whose mass is negligible. As shown in Figure 5, the foot of the table is too small to let the cart remain on the edge of the table. However, if the cart has a proper acceleration, the table can remain upright for a while. At the moment, the ZMP lies inside the table foot. Since the moment around the ZMP must be zero, we have

$$\tau_{zmp} = mg(x - p_x) - m\ddot{x}z_c = 0. \quad (24)$$

A similar cart-table model can also be considered on the y -axis, and we can obtain the same result from eq. (23).

3.2. Walking Pattern Generation

3.2.1. Pattern Generation as an Inverse Problem

When the dynamics of the robot is represented by the cart-table model, it is straightforward to compute the ZMP from a given trajectory of the CoM by substituting the acceleration of the CoM into the ZMP equations. The walking pattern generation is its inverse problem. That is, a trajectory of the CoM should be found from a given ZMP trajectory which can be specified by a sequence of desired foot prints and a period of each step.

Takanishi et al. (1990) applied the fast Fourier transformation (FFT) to a reference trajectory of the ZMP and solved the inverse problem in the frequency domain. A desired trajectory of the CoM can be found by applying inverse FFT to the solution in the frequency domain. Kagami et al. (2000) discretized the ZMP equation in the time domain and transformed the ZMP equations into a trinomial form under a reasonable assumption. The trinomial equations can be solved in $O(N)$ where N is the number of sampling points of the reference trajectory.

Both methods require an entire ZMP reference trajectory of a long period to generate a desired CoM trajectory and should demand an off-line computation as a result. We

propose a novel method that can solve the problem by an on-line computation.

3.2.2. ZMP Control as a Servo Problem

Let us define a new variable

$$u_x = \frac{d}{dt} \ddot{x}, \quad (25)$$

as the time derivative of the horizontal acceleration in the x -direction of the CoM. Introducing u_x as an input, eq. (23) can be transformed into a strictly proper dynamical system as

$$\frac{d}{dt} \begin{bmatrix} x \\ \dot{x} \\ \ddot{x} \end{bmatrix} = \begin{bmatrix} 0 & 1 & 0 \\ 0 & 0 & 1 \\ 0 & 0 & 0 \end{bmatrix} \begin{bmatrix} x \\ \dot{x} \\ \ddot{x} \end{bmatrix} + \begin{bmatrix} 0 \\ 0 \\ 1 \end{bmatrix} u_x, \quad (26)$$

$$p_x = \begin{bmatrix} 1 & 0 & -z_c/g \end{bmatrix} \begin{bmatrix} x \\ \dot{x} \\ \ddot{x} \end{bmatrix}.$$

Equation (22) can also be made strictly proper by introducing u_y in the same way.

The CoM trajectory can be generated by constructing a controller to track the ZMP trajectory as the output of eq. (26). The block diagram of the system is shown in Figure 6. The CoM trajectory can be obtained from state variable x .

Let us examine the system using a simple example. Figure 7 shows an example of ideal trajectories of the ZMP and corresponding CoM for one step of the walking. Suppose that the robot is supported by one leg from 0 to 1.5 s and by another leg from 1.5 to 3.0 s. Then the reference ZMP trajectory should have a step change at 1.5 s and the CoM should have started to move before the event. The system must demand the ZMP reference in the future to realize the case. Although this may sound strange, it does not violate the law of causality. Recall that a car driver looks ahead in the winding road and can determine how to control the steering before curves.

A control using future information was first proposed by Sheridan (1966) and was called “preview control”. Hayase and Ichikawa (1969) developed a linear quadratic (LQ) optimal servo controller based on the same concept. A digital version of the LQ optimal preview controller was developed by Tomizuka and Rosenthal (1979) and was extended to MIMO systems by Katayama et al. (1985), which is applied to our problem.

3.2.3. Pattern Generation by Preview Control

The system of eq. (26) can be discretized with sampling time T as

$$\begin{aligned} \mathbf{x}(k+1) &= \mathbf{A}\mathbf{x}(k) + \mathbf{B}u(k), \\ p(k) &= \mathbf{C}\mathbf{x}(k), \end{aligned} \quad (27)$$

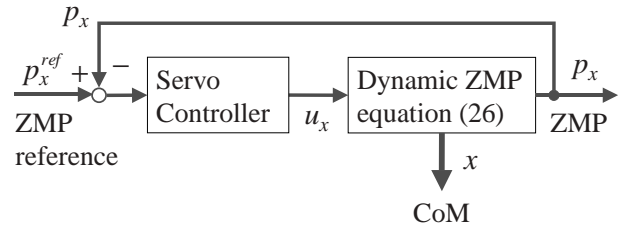


Fig. 6. Pattern generation as ZMP tracking control.

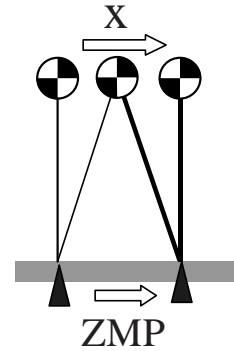
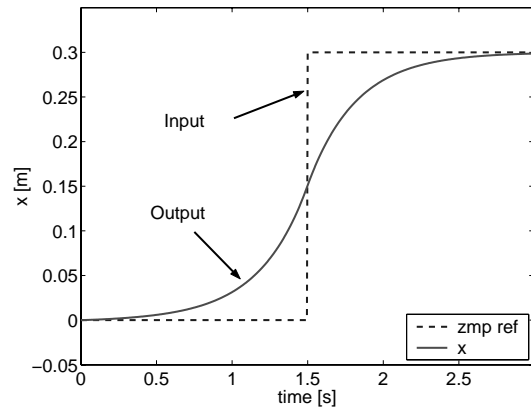


Fig. 7. ZMP and CoM trajectory.

where

$$\begin{aligned} \mathbf{x}(k) &\equiv [x(kT) \quad \dot{x}(kT) \quad \ddot{x}(kT)]^T, \\ u(k) &\equiv u(kT), \\ p(k) &\equiv p_x(kT), \\ \mathbf{A} &\equiv \begin{bmatrix} 1 & T & T^2/2 \\ 0 & 1 & T \\ 0 & 0 & 1 \end{bmatrix}, \\ \mathbf{B} &\equiv \begin{bmatrix} T^3/6 \\ T^2/2 \\ T \end{bmatrix}, \\ \mathbf{C} &\equiv [1 \quad 0 \quad -z_c/g]. \end{aligned}$$

When the reference ZMP $p^{ref}(k)$ is given, the performance index is defined by

$$J = \sum_{i=k}^{\infty} \{Q_e e(i)^2 + \Delta \mathbf{x}^T(i) Q_x \Delta \mathbf{x}(i) + R \Delta u^2(i)\}, \quad (28)$$

where $e(i) \equiv p(i) - p^{ref}(i)$ is the servo error, $Q_e, R > 0$, Q_x is a 3×3 symmetric non-negative definite matrix, $\Delta \mathbf{x}(k) \equiv \mathbf{x}(k) - \mathbf{x}(k-1)$ is the incremental state vector, and $\Delta u(k) \equiv u(k) - u(k-1)$ is the incremental input.

Assuming that the ZMP reference can be previewed for N_L steps in the future at every sampling time, the optimal controller which minimizes the performance index (28) is given by

$$u(k) = -G_i \sum_{i=0}^k e(k) - G_x \mathbf{x}(k) - \sum_{j=1}^{N_L} G_p(j) p^{ref}(k+j), \quad (29)$$

where G_i , G_x , and $G_p(j)$ are the gains calculated from the weights Q_e , Q_x , R and the system parameter of eq. (27).

The preview controller consists of the integration of the tracking error, the state feedback and the preview. Figure 8 shows the gain for the preview. We see the controller does not need the information far in the future because the magnitude of the preview gain G_p becomes very small further than 2 s in the future.

Figure 9 shows an example of the CoM trajectory with the reference ZMP trajectory, generated with the preview period of 1.6 s in the simulation of three steps of forward walking. The upper graph gives the sagittal motion along the x -axis and the lower graph the lateral motion along the y -axis. We can see that a smooth trajectory of the CoM (dashed line) is generated and the resulting ZMP (bold line) follows the reference (thin line) with good accuracy. The ZMP reference is designed to remain in the center of the supporting foot during a single support phase, and to move from the previous supporting foot to the next supporting foot during a double support phase. Cubic spline curves are used to make the ZMP trajectory smooth in the double support phase.

Figure 10 shows the CoM and ZMP trajectories which have been obtained by the preview control with the preview period 0.8 s. The resulted ZMP (bold line) does not follow the reference (thin line) well, and we can observe undershooting in the sagittal motion (x -axis) and overshooting in the lateral motion (y -axis).

3.2.4. Pattern Generation for Multibody Model

The corresponding joint trajectories can be found from the obtained CoM trajectory by solving the inverse kinematics between them, which give a walking pattern. Note that the kinematic equations are non-linear but not differential. The center of the pelvis link can also be used instead of the CoM to reduce the computational complexity.

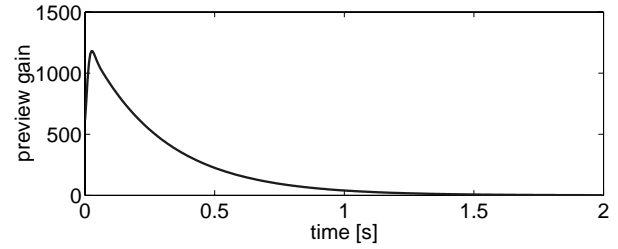


Fig. 8. Preview controller gain G_p ($T = 5$ ms, $z_c = 0.814$ m, $Q_e = 1.0$, $Q_x = 0_{3 \times 3}$, $R = 1.0 \times 10^{-6}$).

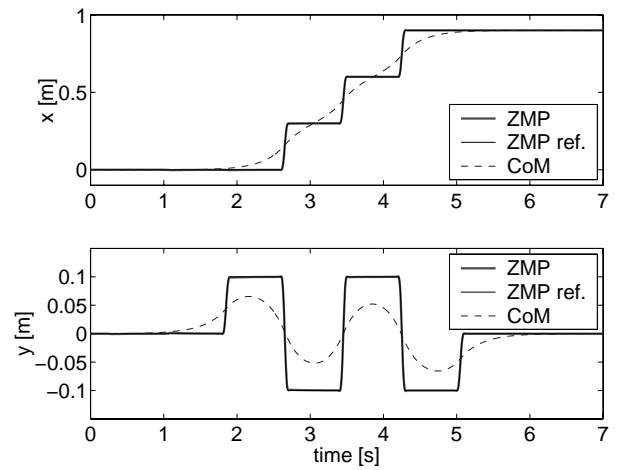


Fig. 9. Body trajectory obtained by preview control, with previewing period $T * N_L = 1.6$ s.

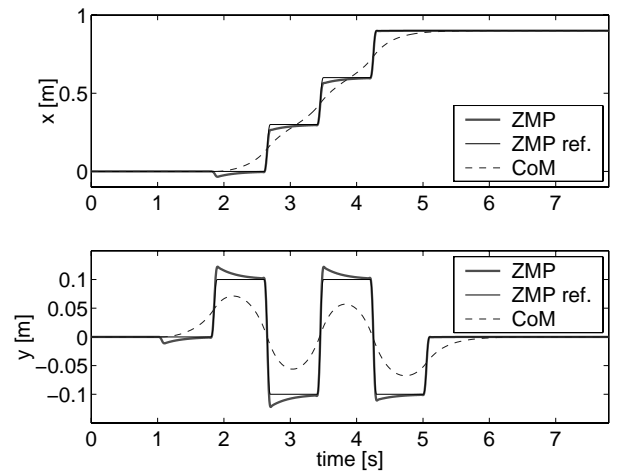


Fig. 10. Body trajectory obtained by preview control, with shorter previewing period $T * N_L = 0.8$ s.

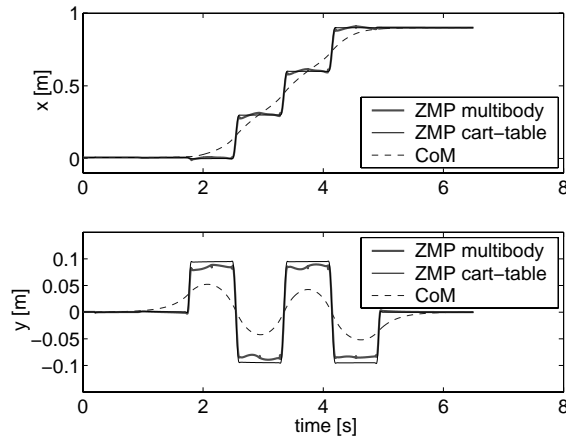


Fig. 11. ZMP calculated by cart-table model and multibody model.

Figure 11 shows the ZMP computed from the cart-table model (thin line) and that from the multibody model (bold line) when the CoM trajectory in Figure 9 is used. The maximum ZMP errors between them were 23 mm in the x -direction and 16 mm in the y -direction, which are relatively large compared with the size of the foot sole of HRP-2P. The error was caused since the cart-table model ignores the angular momentum about the CoM and the center of the pelvis link was used instead of the CoM.

We apply the preview control again to reduce the ZMP error as follows. The CoM trajectory is found from the cart-table model and the expected ZMP error from the multibody model is computed at the same time. Note that the precise ZMP can be found by computing the forward dynamics of the multibody model in real time. The error is stored in a FIFO buffer and used after delay time $T * N_L$. Thus we can use the future ZMP error for the preview control to compensate the ZMP error.

Figure 12 shows the improved ZMP trajectory by the proposed method. We can observe the ZMP of the multibody model (bold line) follows well to the reference ZMP of the cart-table model (thin line). The maximum ZMP error was 12mm in x -direction and 4mm in y -direction which are small enough relative to the size of the foot. The preview period was $T * N_L = 0.75(s)$. This short period was effective enough because the amount of the compensation is small.

3.3. Simulation and Experiment

To demonstrate the performance of the proposed pattern generator, walking on spiral stairs was simulated. The horizontal foot placement was specified so that the foot does not touch the edges of the stairs, and then the horizontal part of the CoM trajectory was generated by the proposed method. Figure 13 shows the generated trajectory. The vertical motion of the

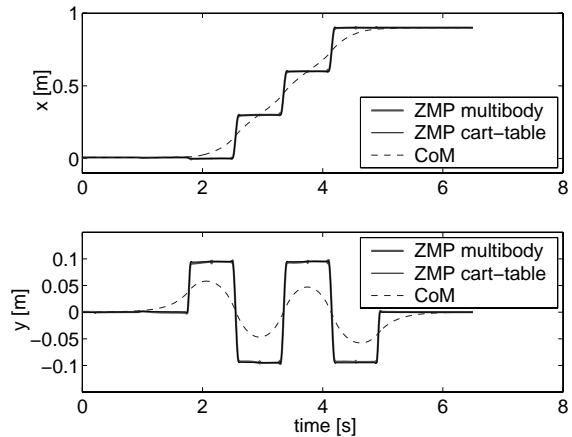


Fig. 12. Modified ZMP of multibody model.

CoM is calculated by the constraint condition (see eq. (10)). Note that the slope of the constraint for each step must be specified from the geometry of the stairs, and all z -intersection (z_c) must be identical.

The dynamic simulation was performed on OpenHRP, which is a dynamics simulator developed in the HRP (Hirukawa, Kanehiro, and Yokoi 2001). Figure 14 shows pictures of the simulated walking and it can be seen that HRP-2P can climb the stairs successfully. The height of each step of the stairs is 0.1 m, the rotation per step is 24° , and the inner radius and outer radius are 0.7 and 1.3 m, respectively.

The average computation time of the pattern generation was 1.1 ms using Intel Xeon CPU 2.8 GHz, including the preview control of the cart-table model (Section 3.2.3) and the compensation for the multibody model (Section 3.2.4). Therefore, the proposed algorithm can generate the walking pattern in real time, since the current implementation of the HRP-2P controller updates the desired joint angles at every 5 ms.

Figure 15 presents photographs of HRP-2P walking, while the proposed method generates the walking pattern in real time. A feedback controller is also applied to realize stable walking (Yokoi et al. 2001). An example of the contact force during the walking is shown in Figure 16.

The proposed pattern generator has been applied to HRP-2P and its improved version HRP-2 in thousands of walking experiments for years, which has confirmed the high performance of the generator. It has also been used by many users of humanoid robot HRP-2, which is commercially available as a research platform.

4. Lying Down and Getting Up

In this section we present how a human-sized humanoid robot that can lie down and get up has been realized in detail.

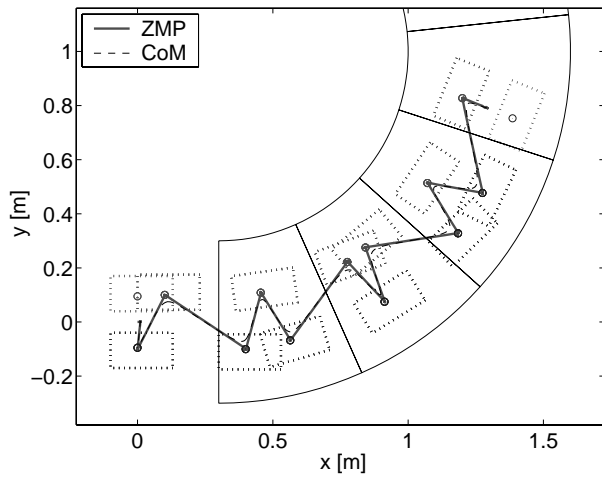


Fig. 13. Planned trajectory for a walk on spiral stairs: ZMP and CoM projected on the horizontal plane.

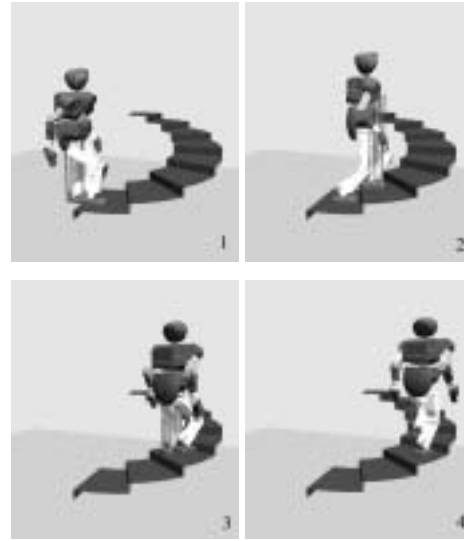


Fig. 14. Pictures of walking on spiral stairs (simulation).

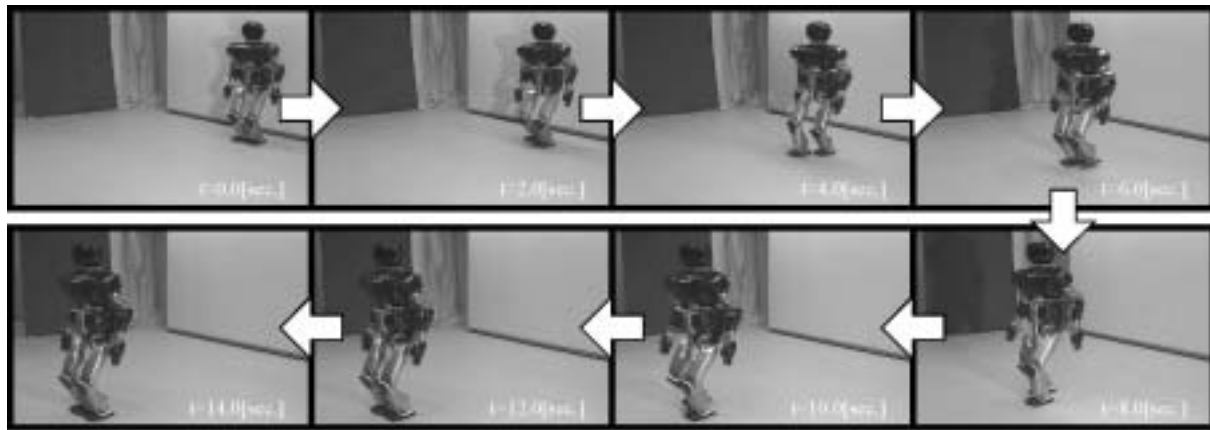


Fig. 15. Bipedal walking of HRP-2P.

4.1. Assumptions

The problem is studied under the following assumptions:

1. the robot gets up from a flat and horizontal plane;
2. the robot lies horizontally on the floor with the face upward or downward;
3. the coefficient of the friction between the robot and the floor is unknown to realize the getting up motion from the floor with any amount of friction.

The proposed method lets neither a hand nor a foot slide on the floor to generate a valid motion under the third assumption.

4.2. Contact State Graph

Getting up is a motion that changes the contact state between the robot and the floor from a state at which its front or back contacts the floor to another state at which its feet contact the floor. The static balance should be kept during a transition from one contact state to another, and the balance is intentionally broken during several transitions. The transitions can be realized by controlling the relationship between the projection of the CoM onto the floor and the supporting polygon of the robot.

From the observation, getting up is segmented into a non-directed graph whose nodes are discrete contact states of the motion as shown in Figure 17. Each contact state is numbered,

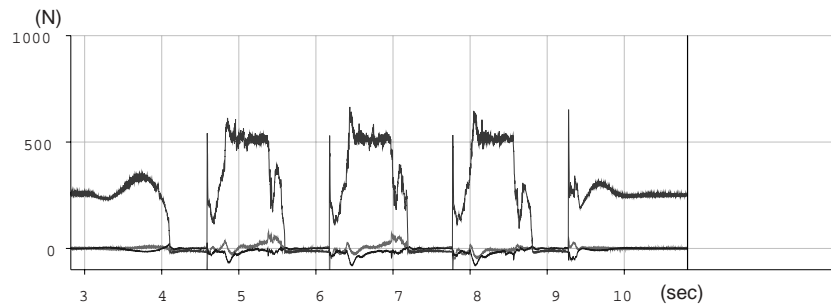


Fig. 16. Contact force during the walking of HRP-2P.

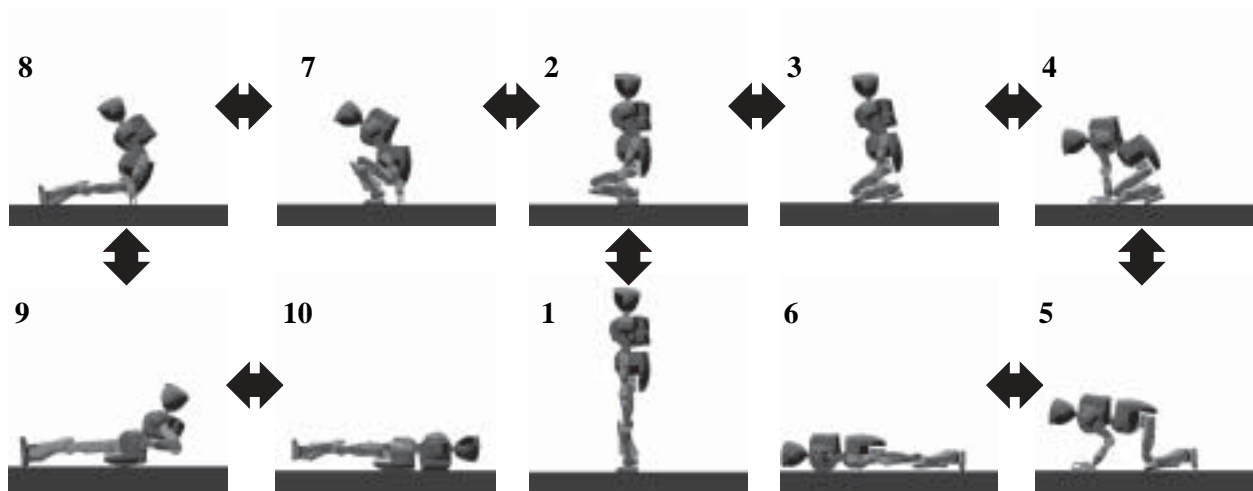


Fig. 17. Contact state graph of getting up.

and the parts of the robot in contact with the floor at each state are shown in Table 2. Although states 1 and 2 have identical contacting parts, state 2 is defined since it is the common state for getting up from lying with the face upward and backward. States 4 and 5 also have identical contacting parts, but the CoM is located at a more forward position in state 5 (see Figure 17).

There are more intermediate states other than the states in the graph. For example, a hand of the robot should leave the floor or the hands and/or knees may not align between states 4 and 5. The robot is in contact with the floor at the toes of the feet between states 2 and 3. The intermediate states are omitted to make the description of the method clear.

It is also possible to let the robot turn over from lying face upward and get up from there with face downward, but the maximum radius of the robot around the yaw axis (z -axis) should be small enough to realize the turn. The radius can be made smaller by having a yaw joint at each shoulder, which is introduced at humanoid robot H7 (Kagami et al. 2001). HRP-2P does not have the joint to make more room in its trunk

Table 2. Support Parts

No.	Support Parts	Support Number	Parts
1	Sole	6	Chest and toe
2	Sole	7	Sole and finger
3	Knee and toe	8	Heel and finger
4	Wrist, knee and toe	9	Hip and heel
5	Wrist, knee and toe	10	Back and hip

for removing a possible backpack and the mechanism of the arms is more rigid. This is why we tried to realize the motions based on the contact state graph shown in Figure 17.

4.3. Transitions Among the Contact States

Most transitions among the contact states can be realized by quasi-static motions. That is, the projection of the CoM onto the floor can remain in the supporting polygon of the robot

during the transition motions. The exceptional case is the transition between states 2 and 3. The robot must rotate about the toes of the feet during the transition, during which the projection of the CoM may not be in the supporting polygon. The rotational motion is required since the robot cannot contact the floor at the knees and the soles due to the small movable range of the angle joints.

The quasi-static motions are executed as follows. The corresponding motions of the robot are generated in an off-line way to move the CoM by controlling the trunk while keeping the contact state. For example, the transition from states 2 to 7 can be realized by tilting the trunk to let the hands touch the floor while keeping the projection of the CoM inside the feet. Then the tips of the hands can also support the robot. While the planned motion is executed, the orientation of the trunk is estimated from the gyroscope and the accelerometer mounted on the robot using a Kalman filter, and the relationship between the projection of the CoM and the supporting polygon is monitored to check if the execution is going on as planned. Although it is also possible to modify the motion by the sensor data, most motions use the whole movable ranges of many joints during the transitions and therefore the feedback control is difficult to apply.

The dynamic motion can be executed as follows. The transition from states 2 to 3 and from states 3 to 2 are reversible in principle; the transition from states 3 to 2 is described. The transition consists of three phases. In phase 1, the hip pitch joints are moved to follow a sinusoidal wave

$$\theta_{hip}(t) = \theta_{hip}(0) - A_{hip}[\cos(\omega t) - 1], \quad (30)$$

for swinging the upper body backward. An inertia force is generated, where θ_{hip} is the desired joint angle of the hip pitch joint $\theta_{hip}(0)$ is the initial value of the angle corresponding to the joint angle at state 3, and A_{hip} is the magnitude of the curve. Letting θ_{body} be the estimated orientation of the trunk about the pitch axis from the Kalman filter, the angle between the soles and the floor can be given by

$$\theta_{sole}(t) = \theta_{body}(t) + \theta_{hip}(t) + \theta_{knee}(t) + \theta_{ankle}(t), \quad (31)$$

where θ_{knee} and θ_{ankle} are the joint angles of the knees and the ankles, respectively. When the inequality

$$\theta_{sole}(t) < \theta_{sole}(0) - \theta_{sole}^0 \quad (32)$$

holds, the algorithm judges that the robot starts to rotate about the toe axis, where $\theta_{sole}(0)$ is the initial orientation of the soles at state 3 and θ_{sole}^0 is a threshold to judge enough inertia force has been generated for keeping the rotation.

In phase 2, an interpolating motion from the current joint angles to the initial joint angles of state 2 is executed while a feedback control is applied to prevent the robot from falling backward due to the landing impact to the soles and the generated inertia force. The feedback control can make the ZMP

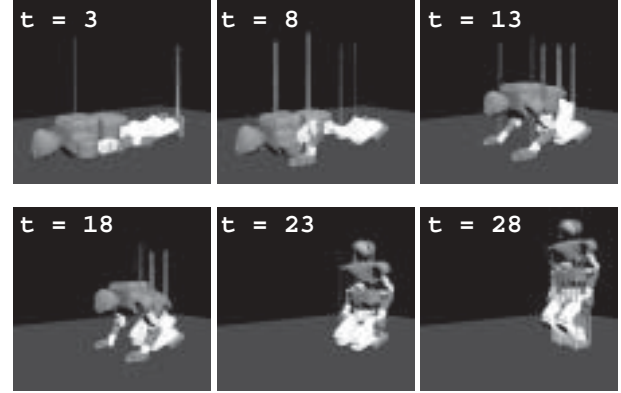


Fig. 18. Standing up motion simulation (units are seconds).

follow the desired trajectory and the position of the trunk remain at that of state 2. The control moves the trunk horizontally by rotating the ankle joints and the hip joints to opposite directions with the same amount. The joint angle $\tilde{\theta}$ for the feedback control can be found by

$$\Delta P(t_i) = P_d(t_i) - P(t_i), \quad (33)$$

$$\tilde{\theta}(t_i) = k_1 \Delta P(t_i) + k_2 \tilde{\theta}(t_{i-1}), \quad (34)$$

where $P_d(t_i)$ is the desired position of the ZMP at t_i and is set to the middle of the soles here, $P(t_i)$ is the current position of the ZMP found from the six-axis force sensor mounted at the ankles, and $0 < k_1$ and $0 < k_2 < 1$ are the feedback gains. $\tilde{\theta}$ is added to the ankle joint angle and subtracted from the hip joint angle found by the interpolation.

In phase 3, the feedback control is applied to keep the state.

4.4. Application to HRP-2P

4.4.1. Simulation

The proposed method is implemented on OpenHRP, and an example of the simulation is shown in Figure 18. The simulations were executed before HRP-2P was designed. The results of the simulations found the required torque for the joints to realize the motions, and the specifications of the motors and the reduction mechanism were determined then. For example, the trajectories of the torque of the hip pitch joint, the knee joint, the ankle pitch joint, and the waist pitch joint when the robot gets up from lying face downward are shown in Figure 19.

4.5. Experiment

Figure 21 shows photographs of HRP-2P getting up. Figure 21 shows HRP-2P getting up from lying face downward, and

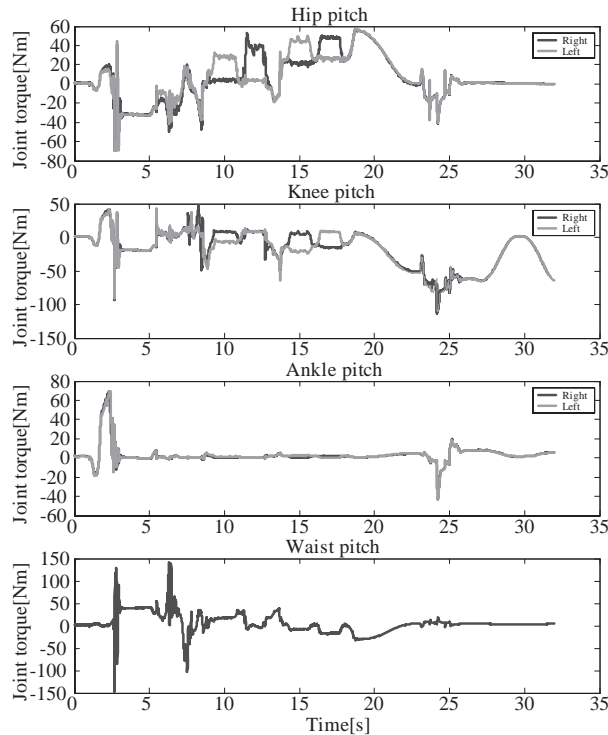


Fig. 19. Joint torques during standing up motion.

Figure 22 shows HRP-2P face upward. The photographs were taken every 5 s, and the whole motions required about 30 s. Figure 20 shows the trajectories of θ_{hip} , θ_{sole} , $\Delta P(t)$, and $\tilde{\theta}(t)$ during the transition from states 3 to 2.

The horizontal dashed lines in the graph of $\Delta P(t)$ denote the position of the toe and the heel, respectively. The ZMP is located at the toe at the initial state since the robot is supported at the toes. θ_{hip} was controlled by eq. (30) in phase 1, where $\omega = 3.14$, $A_{hip} = 3.0^\circ$. The horizontal dashed lines in the graph of θ_{sole} denote θ_{sole0} and $\theta_{sole} - \theta_{sole_thd}$. The rotation about the toe axis was detected at $t = 1.0$ when θ_{sole} was lower than the line. The ZMP still remained at the toe during the rotation about the toe, and $\Delta P(t)$ started to move around $t = 1.5$, since the soles touched the floor. After the landing, the ZMP moved to the heel at $t = 2.0$ because of the generated inertia force and the impact force at the landing. $\Delta P(t)$ approached zero by the feedback control, where $k_1 = 0.06$ and $k_2 = 0.01$.

The lying down of HRP-2P was also realized as the inverse motion of the corresponding getting up based on the contact state graph in Figure 17, as shown in Figures 23 and 24.

5. Conclusions

The contributions of the paper are summarized as follows.

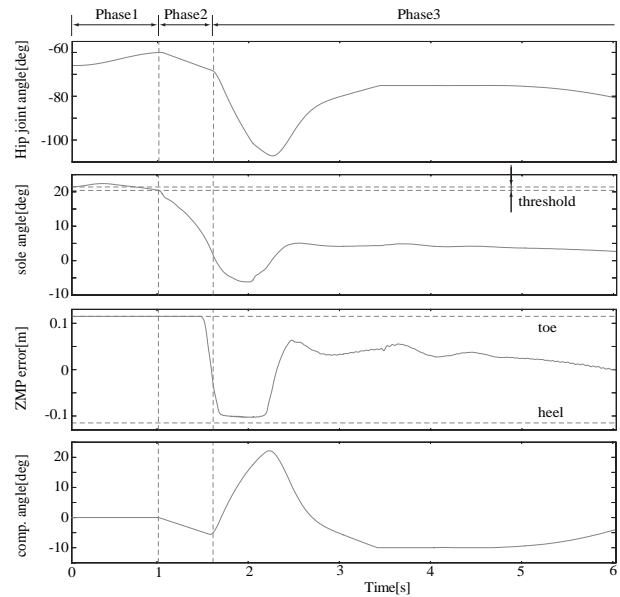


Fig. 20. θ_{hip} , θ_{sole} , $\Delta P(t)$, and $\tilde{\theta}(t)$ during the transition from state 3 to state 2.

- We have developed a human-size humanoid robot which is free from a large backpack and has joints with wide movable ranges including waist joints.
- We have proposed a novel method for biped walking pattern generation. We formalized the problem as the design of a ZMP tracking servo controller. It was shown that we can design such a controller by adopting the preview control that uses the future ZMP reference.
- It has also been shown that a preview controller can be used to compensate the ZMP error caused by the difference between the simple cart-table model and the precise multibody model. To demonstrate the proposed method, a walking pattern for spiral stairs was generated and verified by dynamic simulation. The motion pattern was also successfully applied to HRP-2P walking.
- We have proposed to segment the motions into a collection of discrete contact states and to represent them by the undirected graph. The controllers have been designed to realize the transitions between the contact states.
- We have also presented how the transitions between the contact states can be realized by the dynamic control.

The proposed walking pattern generator has been used in thousands of walking experiments of the humanoid robot HRP-2, and has been used by many users of HRP-2, which

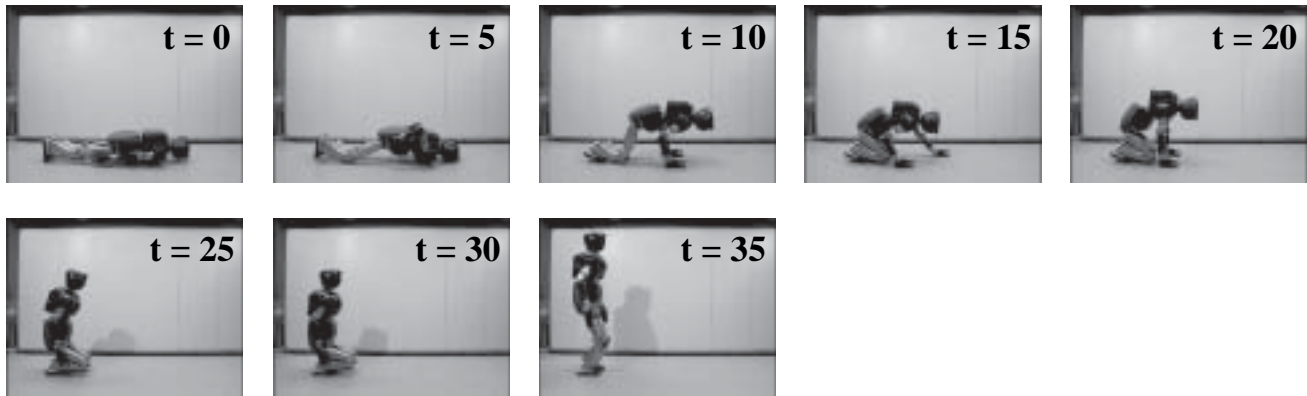


Fig. 21. The state of the getting up motion from lying face down (units are seconds).

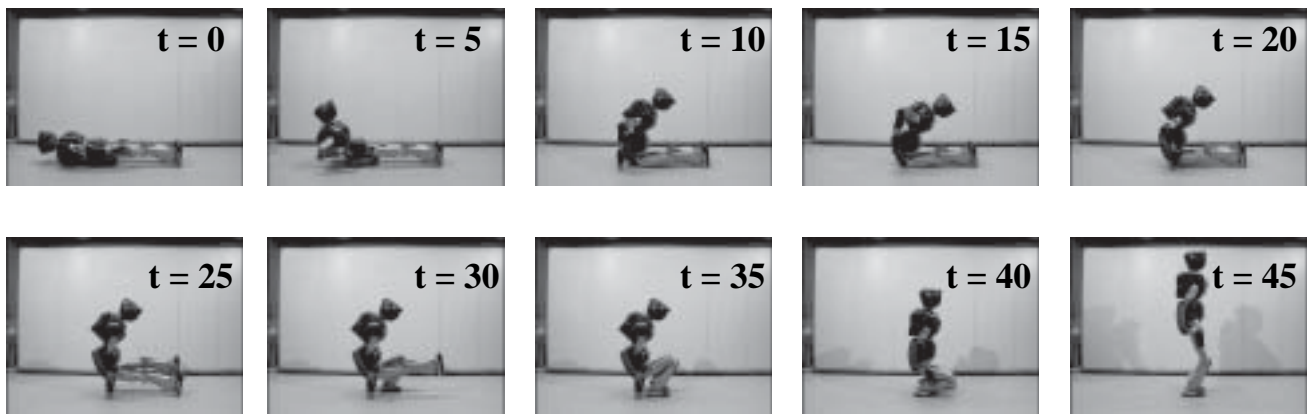


Fig. 22. The state of the getting up motion from lying on the back (units are seconds).

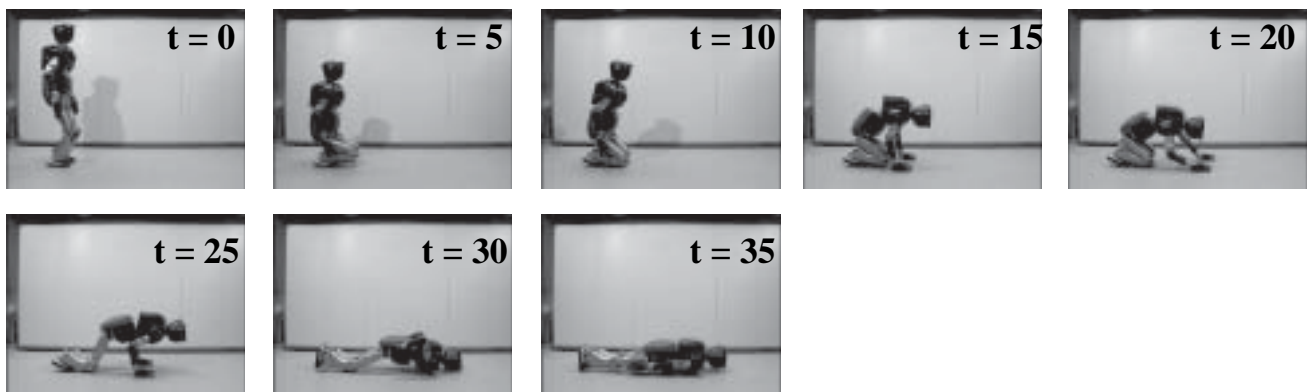


Fig. 23. Lying down motion with the face downward (units are seconds).

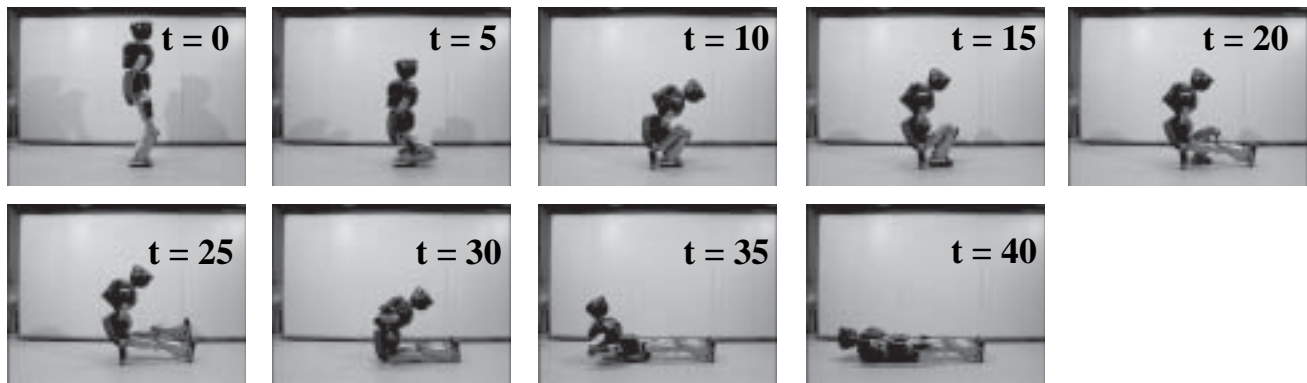


Fig. 24. Lying down motion with the face upward (units are seconds).

has been commercially available as a research platform. The falling motion control to realize “safe falling down” is another important building block towards a useful humanoid robot in a real environment (Fujiwara et al. 2002).

Acknowledgments

This research was supported by the HRP of METI, Japan, partly through the New Energy and Industrial Technology Development Organization (NEDO) and the Manufacturing Science and Technology Center (MSTC).

References

- Fujiwara, K., Kanehiro, F., Kajita, S., Kaneko, K., Yokoi, K., and Hirukawa, H. 2002. UKEMI: falling motion control to minimize damage to biped humanoid robot. *Proceedings of the IEEE/RSJ International Conference on Intelligent Robotics and Systems (IROS'02)*, EPFL, Lausanne, Switzerland, September 30–October 4.
- Furuta, T., Okumura, Y., Tawara, T., and Kitano, H. 2001. “morph”: a small-size humanoid platform for behavior coordination research. *Proceedings of the 2nd IEEE-RAS International Conference on Humanoid Robots*, Tokyo, Japan, November 22–24, pp. 165–171.
- Gienger, M. et al. 2001. Toward the design of a biped jogging robot. *Proceedings of the IEEE International Conference on Robotics and Automation (ICRA)*, Seoul, Korea, May 21–26, pp. 4140–4145.
- Hara, K., Yokogawa, R., and Sadao, K. 1997. Dynamic control of biped locomotion robot for disturbance on lateral plane. *Proceedings of the Japan Society of Mechanical Engineers 72nd Kansai Meeting*, pp. 10-37–10-38 (in Japanese).
- Hayase, M. and Ichikawa, K. 1969. Optimal servosystem utilizing future value of desired function. *Transactions of SICE* 5(1):86–94 (in Japanese).
- Hirai, K., Hirose, M., Haikawa, Y., and Takenaka, T. 1998. The development of Honda Humanoid Robot. *Proceedings of the 1998 IEEE International Conference on Robotics and Automation (ICRA)*, Leuven, Belgium, pp. 1321–1326.
- Hirose, M., Haikawa, Y., Takenaka, T., and Hirai, K. 2001. Development of Humanoid Robot ASIMO. *Proceedings of the IEEE/RSJ International Conference on Intelligent Robots and Systems, Workshop 2*, Maui, HI, October.
- Hirukawa, H., Kanehiro, F., and Yokoi, K. 2001. HRP develops OpenHRP. *Proceedings of the IEEE/RSJ International Conference on Intelligent Robots and Systems, Workshop on Explorations towards Humanoid Robot Applications*, Maui, HI, October.
- Huang, Q., Yokoi, K., Kajita, S., Kaneko, K., Arai, H., Koyachi, N., and Tanie, K. 2001. Planning walking patterns for a biped robot. *IEEE Transactions on Robotics and Automation* 17(3):280–289.
- Inaba, M., Kanehiro, F., Kagami, S., and Inoue, H. 1995a. Two-armed bipedal robot that can walk, roll-over and stand up. *Proceedings of the IEEE/RSJ International Conference on Intelligent Robots and Systems*, Munich, Germany, pp. 297–302.
- Inaba, M., Kanehiro, F., Kagami, S., and Inoue, H. 1995b. Vision-equipped apelike robot based on the remote-brained approach. *Proceedings of the IEEE International Conference on Robotics and Automation (ICRA)*, Nagoya, Japan, pp. 2193–2198.
- Inoue, H., Tachi, S., Nakamura, Y., Ohyu, N., Hirai, S., Tanie, K., Yokoi, K., and Hirukawa, H. 2001. Overview of Humanoid Robotics Project of METI. *Proceedings of the 32nd International Symposium on Robotics (ISR)*, Seoul, Korea, April, 19–21.
- Kagami, S., Nishiwaki, K., Kitagawa, T., Sugihara, T., Inaba, M., and Inoue, H. 2000. A fast generation method of a dynamically stable humanoid robot trajectory with enhanced ZMP constraint. *Proceedings of the 1st IEEE-RAS International Conference on Humanoid Robots*, MIT, Cambridge, MA, September 7–8.
- Kagami, S., Nishiwaki, K., Kuffner, J. J. Jr., Kuniyoshi, Y., Inaba, M., and Inoue, H. 2001. Design and implementa-

- tion of software research platform for humanoid robots: H7. *Proceedings of the 2nd IEEE-RAS International Conference on Humanoid Robots*, Tokyo, Japan, November 22–24, pp. 253–258.
- Kajita, S. and Tani, K. 1991. Study of Dynamic Biped Locomotion on Rugged Terrain. *Proceedings of the IEEE International Conference on Robotics and Automation (ICRA)*, Sacramento, CA, pp. 1405–1410.
- Kajita, S., Matsumoto, O., and Saigo, M. 2001. Real-time 3D walking pattern generation for a biped robot with telescopic legs. *Proceedings of the IEEE International Conference on Robotics and Automation (ICRA)*, Seoul, Korea, May 21–26, pp. 2299–2308.
- Kajita, S., Kanehiro, F., Kaneko, K., Fujiwara, K., Yokoi, K., and Hirukawa, H. 2002. A real-time pattern generator for biped walking. *Proceedings of the IEEE International Conference on Robotics and Automation (ICRA)*, Washington, DC, May 11–15, pp. 31–37.
- Kanehiro, F., Fujiwara, K., Kajita, S., Yokoi, K., Kaneko, K., Hirukawa, H., Nakamura, Y., and Yamane, K. 2002. Open architecture humanoid robotics platform. *Proceedings of the IEEE International Conference on Robotics and Automation (ICRA)*, Washington, DC, May 11–15, pp. 24–30.
- Kaneko, K., Kajita, S., Kanehiro, F., Yokoi, K., Fujiwara, K., Hirukawa, H., Kawasaki, T., Hirata, M., and Isozumi, T. 2002a. Design of advanced leg module for Humanoid Robotics Project of METI. *Proceedings of the IEEE International Conference on Robotics and Automation (ICRA)*, Washington, DC, May 11–15, pp. 38–45.
- Kaneko, K., Kanehiro, F., Kajita, S., Yokoyama, K., Akachi, K., Kawasaki, T., Ota, S., and Isozumi, T. 2002b. Design of prototype humanoid robotics platform for HRP. *Proceedings of the IEEE/RSJ International Conference on Intelligent Robots and Systems (IROS)*, EPFL, Lausanne, Switzerland, September 30–October 4.
- Katayama, T., Ohki, T., Inoue, T., and Kato, T. 1985. Design of an Optimal Controller for a Discrete Time System Subject to Previewable Demand. *International Journal of Control* 41(3):677–699.
- Kuroki, Y., Ishida, T., Yamaguchi, J., Fujita, M., and Doi, T. T. 2001. A small biped entertainment robot. *Proceedings of the 2nd IEEE-RAS International Conference on Humanoid Robots*, Tokyo, Japan, November 22–24, pp. 181–186.
- Nishiwaki, K., Sugihara, T., Kagami, S., Kanehiro, F., Inaba, M., and Inoue, H. 2000. Design and development of research platform for perception-action integration in humanoid robot: H6. *Proceedings of the IEEE/RSJ International Conference on Intelligent Robotics and Systems (IROS)*, Takamatsu, Japan, October 30–November 5.
- Pratt, J., Dilworth, P., and Pratt, G. 1997. Virtual model control of a bipedal walking robot. *Proceedings of the IEEE International Conference on Robotics and Automation (ICRA)*, Albuquerque, NM, pp. 193–198.
- Raibert, M., Kuroki, Y., Playter, R., Ishida, T., and Doi, T. 2001. Dynamics simulation of humans and humanoids. *Proceedings of the 2nd IEEE-RAS International Conference on Humanoid Robots*, Tokyo, Japan, November 22–24, pp. 265–270.
- Sano, A. and Furusho, J. 1990. Realization of natural dynamic walking using the angular momentum information. *Proceedings of the IEEE International Conference on Robotics and Automation (ICRA)*, Cincinnati, OH, Vol. 3, pp. 1476–1481.
- Sheridan, T. B. 1966. Three models of preview control. *IEEE Transactions on Human Factors in Electronics* 7(2):91–102.
- Sugihara, T., Nakamura, Y., and Inoue, H. 2002. Real-time humanoid motion generation through ZMP manipulation based on inverted pendulum control. *Proceedings of the IEEE International Conference on Robotics and Automation (ICRA)*, Washington, DC, May 11–15, pp. 1404–1409.
- Takanishi, A., Lim, H., Tsuda, M., and Kato, I. 1990. Realization of dynamic biped walking stabilized by trunk motion on a sagittally uneven surface. *Proceedings of the IEEE International Workshop on Intelligent Robots and Systems (IROS)*, pp. 323–330.
- Tomizuka, M. and Rosenthal, D. E. 1979. On the optimal digital state vector feedback controller with integral and preview actions. *Transactions of the ASME, Journal of Dynamic Systems, Measurement and Control* 101:172–178.
- Vukobratović, M. and Stepanenko, J. 1972. On the stability of anthropomorphic systems. *Mathematical Biosciences* 15:1–37.
- Yamaguchi, J., Soga, E., Inoue, S., and Takanishi, A. 1999. Development of a bipedal humanoid robot-control method of whole body cooperative dynamic biped walking. *Proceedings of the IEEE International Conference on Robotics and Automation (ICRA)*, Detroit, MI.
- Yamasaki, F., Matsui, T., Miyashita, T., and Kitano, H. 2000. PINO: the humanoid that walks. *Proceedings of the 1st IEEE-RAS International Conference on Humanoid Robots*, MIT, Cambridge, MA, September 7–8.
- Yokoi, K., Kanehiro, F., Kaneko, K., Fujiwara, K., Kajita, S., and Hirukawa, H. 2001. A Honda humanoid robot controlled by AIST software. *Proceedings of the 2nd IEEE-RAS International Conference on Humanoid Robots*, Tokyo, Japan, November 22–24.